Effect of the SNR Model in the Performance Assessment of Cooperative Spectrum Sensing

Luiz Renault Leite Rodrigues and Dayan Adionel Guimarães

Abstract— **This work investigates the impact of different signal-to-noise ratio (SNR) models on the performance assessment of spectrum sensing algorithms under varying signal and noise levels. Through analytical derivation and simulations, we demonstrate that the choice of SNR model can significantly influence perceived detection performance, particularly in environments with random noise power. Our results highlight that using an inadequate or poorly described SNR model can lead to inaccurate conclusions. These findings emphasize the critical importance of both selecting an appropriate SNR model and clearly stating it when evaluating spectrum sensing systems.**

Keywords— **Cognitive radio, cooperative spectrum sensing, dynamic spectrum access, signal-to-noise ratio.**

I. Introduction

Spectrum sensing is a fundamental component in cognitive radio (CR) networks, playing a critical role in identifying vacant frequency bands to enable dynamic spectrum access (DSA). Accurate assessment of spectrum availability ensures optimal utilization of limited spectral resources and prevents harmful interference with licensed primary users (PUs).

Various models have been proposed in the literature to characterize the received signal and the noise at a CR receiver, each with distinct implications for evaluating the effectiveness of spectrum sensing algorithms. The choice of appropriate models significantly impacts performance metrics such as detection probability, false alarm rate, and overall system efficiency. Common signal models range from simplified theoretical assumptions, such deterministic models, to more complex, realistic statistical models, representing different environmental conditions and propagation characteristics, which in turn influence the accuracy of sensing outcomes.

This work investigates how the signal-to-noise (SNR) model may substantially affect the performance assessment of spectrum sensing algorithms. Through both analytical reasoning and simulation-based experiments, we show that different SNR definitions can lead to divergent conclusions about algorithm effectiveness.

A. Related Work

Numerous studies have emphasized the critical role of the SNR in the performance evaluation of spectrum sensing algorithms. A foundational contribution is the concept of the SNR wall, which establishes a lower bound on detection performance in the presence of noise uncertainty [1].

The impact of fading channels on detection performance has also been extensively studied. For instance, in [2] the behavior of energy detection across various fading environments was analyzed, including additive white Gaussian noise (AWGN), Rayleigh, Nakagami-m, and Rician channels. The findings confirm that detection probability is strongly influenced by the underlying channel characteristics.

Cooperative spectrum sensing (CSS) has been proposed to mitigate the limitations of individual sensors in low-SNR regimes. However, [3] indicates that CSS may offer only marginal improvements when the SNR is below critical thresholds, especially if noise variability is not properly modeled.

To address the variability of real-world conditions, advanced approaches have emerged that incorporate SNR estimation and adaptation. In particular, multistage sensing schemes such as those proposed by [4] adapt their detection strategies based on estimated SNR values, showing pronounced improvements in both detection accuracy and computational efficiency. These approaches rely heavily on the reliability of the SNR model.

Recent studies have also increasingly acknowledged that the noise power in wireless environments is often random, which directly impacts the reliability of spectrum sensing performance evaluations. In [5], the authors design a detector under the assumption that noise is a random process with unknown characteristics, without precisely defining the resulting SNR. Similarly, the work in [6] models the noise variance as an uncertain and varying quantity, leading to a performance evaluation framework where the actual SNR is not fixed, but implicitly dependent on a range of possible noise power values. In [7], the detection method deliberately avoids relying on a known noise power, effectively operating without an explicit SNR definition. Likewise, [8] employs a dynamic noise floor estimation technique, acknowledging that noise power changes over time and that any fixed SNR assumption would be unrealistic.

Despite the demonstrated influence of SNR modeling on spectrum sensing assessment, a significant number of publications either do not specify the adopted SNR model or implicitly assume deterministic conditions. This omission can lead to inconsistent or misleading performance comparisons across studies.

B. Problem Description

Let $P_{RX}, P_N \geq 0$ be random variables representing the instantaneous powers of the received signal and noise, respec-

Luiz R. L. Rodrigues, Inatel, Santa Rita do Sapucaí, e-mail: luiz.rodrigues@dtel.inatel.br; Dayan A. Guimarães, Inatel, Santa Rita do Sapucaí, e-mail: dayan@inatel.br. This work was funded by resources from the following agencies: RNP/MCTI (Grant 01245.010604/2020-14), EMBRAPII/MCTI (Grants 052/2023 PPI IoT/Manufatura 4.0, PPE-00124-23), FAPESP (Grants 22/09319-9, 20/05127-2), FAPEMIG (Grants APQ-04523-23, APQ-05305-23, APQ-01558-24, RED-00194-23), and CNPq (Grant 302589/2021-0).

tively. We consider two models for defining the SNR:

$$\text{SNR}_1 = \frac{\mathbb{E}[P_{RX}]}{\mathbb{E}[P_N]}, \text{ and } \text{SNR}_2 = \mathbb{E}\left[\frac{P_{RX}}{P_N}\right],$$

denoted respectively as Model 1 and Model 2. In general terms, Model 1 defines the SNR as the ratio between the expected signal power and the expected noise power, and Model 2, in contrast, defines the SNR as the expected value of the instantaneous signal-to-noise power ratio.

Assuming that P_{RX} and P_N are independent, Model 2 becomes

$$\text{SNR}_2 = \mathbb{E}[P_{RX}]\mathbb{E}\left[\frac{1}{P_N}\right].$$

The two models yield identical values only when $\mathbb{E}\left[1/P_N\right] = 1/\mathbb{E}[P_N]$, which holds true if P_N is deterministic. Otherwise, due to the convexity of the reciprocal function and Jensen's inequality, we have

$$\mathbb{E}\left[\frac{1}{P_N}\right] \geq \frac{1}{\mathbb{E}[P_N]} \quad \Rightarrow \quad \text{SNR}_2 \geq \text{SNR}_1.$$

To understand the implications of this inequality, four scenarios are considered: i) Both P_{RX} and P_N are random, yielding $\text{SNR}_2 \geq \text{SNR}_1$. ii) Both $P_{RX} = p_{RX_0}$ and $P_N = p_{N_0}$ are constant, yielding $\text{SNR}_1 = \text{SNR}_2 = p_{RX_0}/p_{N_0}$. iii) P_{RX} is random and $P_N = p_{N_0}$ is constant, also yielding $\text{SNR}_1 = \text{SNR}_2 = \mathbb{E}[P_{RX}]/p_{N_0}$. iv) $P_{RX} = p_{RX_0}$ is deterministic and P_N is random, yielding $\text{SNR}_2 \geq \text{SNR}_1$.

These results show that the choice of SNR model can affect performance assessments whenever the noise power is random - a typical case in wireless systems subject to hardware variability or environmental effects. Surprisingly, many works in the literature do not explicitly define which SNR model they use, leading to ambiguities and difficulties in comparing results across studies.

C. Contributions and organization of the article

Our goal in this work is to quantify the discrepancies that may arise in the performance of spectrum sensing algorithms when different SNR models are assumed, filling the gap in the literature concerning proper SNR modeling and consequences.

As a byproduct, simulation files were made publicly available[1] to aid future comparisons in spectrum sensing algorithm performance and SNR model effects.

The remaining of paper is organized as follows. Section II presents the definitions for the system model, which includes the primary user signal, channel and noise models, SNR expressions for the system model, and the detector algorithms. The numerical results are presented in Section III, and Section IV summarizes the findings and proposes additional topics for further investigations.

II. System Model

The network and system model are based on [9]. The network topology is formed by a set of m secondary users (SUs) distributed uniformly on a circular region with radius r, centered at $(0, 0)$, and a fixed PU transmitter located at (PU_x, PU_y).

[1]The source code is available at github.com/luizrenault/snrmodel

A signal is transmitted from the PU with power P_{TX}, and is affected by the wireless channel, producing a received signal with power P_{RX_i}, which is then added to a noise signal with power P_{N_i}, resulting in a signal-to-noise ratio SNR_i, $i = 1, \ldots, m$, for each ith SU, before presented to the spectrum sensing algorithm for the spectrum occupancy inference. The model components are described as follows.

A. Signal Model

The transmitted signal is composed by n complex samples representing a quaternary phase-shift keying (QPSK) modulation scheme with N_s samples per symbol and a sample rate of $1/T_s$. This results in a $n \times 1$ signal vector $\mathbf{x}$, encompassing n/N_s transmitted symbols. In this sense, the average transmitted signal power can be calculated by $\overline{P_{TX}} = \frac{1}{n}\sum_{j=1}^{n}\left|x_{TX_j}\right|^2$, with x_{TX_j}, $j = 1, \ldots, n$ being the individual complex samples and $|\cdot|$ denoting the absolute value operator.

B. Channel Model

As in [9], the channel model incorporates distance-dependent received signal levels, spatially correlated shadowing and multipath fading characterized by an environment-dependent random Rice factor.

The channel affects the transmitted signal as a complex gain that changes both magnitude and phase of the signal samples.

Let $\mathbf{h}$ be the $m \times 1$ channel gain vector with elements given by $h_i = g_i^{1/2} s_i^{1/2} a_i$, where $g_i = (d_0/d_i)^\eta$ is the real gain for the log-distance path loss model, d_0 is the reference distance in which the transmitted signal power P_{TX} is known, d_i is the exact distance from the PU to the ith SU, η is a dimensionless, environment-dependent path loss exponent, s_i is the spatially correlated shadowing gain, and $a_i = \mathbb{CN}(\sqrt{K_i/(K_i+1)}, 1/(K_i+1))$ is a complex Gaussian random variable, with $K_i = 10^{K_i^{\text{dB}}/10}$ and K_i^{dB} being the Rice factor in dB for the particular channel formed by the PU and the ith SU, modeled as a real Gaussian random variable with mean μ_K^{dB} and standard deviation σ_K^{dB}, which are determined according to the environmental characteristics.

The gain $s_i = 10^{s_i^{\text{dB}}/10}$ models the log-normal signal shadowing component that affects the ith SU. It is modeled as a Gaussian random variable with zero mean and standard deviation σ_s^{dB}, also dependent on the environment. The realization of a specific value of s_i^{dB} to achieve the spatial correlation requirements is detailed as follows.

The circular SU coverage area is circumscribed by a square region divided into $v \times v$ small squares (sub-regions) with sides equal to $2r/v$. For each sub-region, a shadowing gain $s_{c_{x,y}}^{\text{dB}}$, $x, y = 1, \ldots, v$, is computed using $\mathbf{S}_\mathbf{c}^{\text{dB}} = \mathbf{L}\mathbf{S}_\mathbf{u}^{\text{dB}}\mathbf{L}^{\text{T}}$, where $\mathbf{S}_\mathbf{c}^{\text{dB}}$ is the matrix formed by the elements $s_{c_{x,y}}^{\text{dB}}$, $\mathbf{S}_\mathbf{u}^{\text{dB}}$ is a $v \times v$ matrix with zero-mean uncorrelated Gaussian samples with standard deviation σ_s^{dB}, $\mathbf{L}$ is the lower triangular matrix from the Cholesky decomposition of the matrix $\mathbf{\Sigma}$ described below, and $[\cdot]^{\text{T}}$ denotes matrix or vector transposition.

The matrix $\mathbf{\Sigma} \in \mathbb{R}^{v \times v}$ is constructed using the negative-exponential correlation model, having elements $\Sigma_{x,y}$ =

$\exp(-\delta_{x,y}/\Lambda)$, where $\delta_{x,y} = |x-y|\sqrt{2}$ is the distance between the matrix elements indexed by (x, y) and the diagonal, and Λ is the correlation length. The value of S_i is selected based on the sub-region where the ith SU lies [9].

The resulting signal samples at the input of the SU receiver are given by $x_{RX_{i,j}} = h_i x_{TX_j}$, $i = 1, \dots, m$, $j = 1, \dots, n$, which are arranged on the $m \times n$ matrix $\mathbf{X}_{\text{RX}} = \mathbf{h}\mathbf{x}^{\text{T}}$.

C. Noise Model

In order to model the inherent differences between physical receivers and undesired random interfering signals on the surroundings (discerned as noise), a non-uniform time-variant noise is considered herein.

Let $\mathbf{W}$ be the $m \times n$ noise matrix with elements $w_{i,j}$, $i = 1, \dots, m$, $j = 1, \dots, n$, which are complex noise samples in the ith SU receiver. It is assumed that $w_{i,j}$ are zero mean Gaussian random variables with variance $\sigma_i^2 = (1 + \rho u_i)\overline{\sigma}^2$, where $\overline{\sigma}^2$ is the average noise variance across all SUs, $0 \leq \rho < 1$ is the parameter that accounts for the fractional variation of the noise power around the average $\overline{\sigma}^2$, and u_i is a uniform random variable in $[-1, 1]$, evaluated for each SU. Then, the noisy received samples are given by $\mathbf{X} = \mathbf{X}_{\text{RX}} + \mathbf{W}$.

D. SNR Models

The SNR models described in Section I-B can be particularized for this system model as shown in what follows.

$$\text{SNR}_1 = \frac{\mathbb{E}[P_{RX}]}{\mathbb{E}[P_N]}, \text{with}$$
$$\mathbb{E}[P_{RX}] = \overline{P_{TX}}\mathbb{E}\left[\left(\frac{d_0}{d_i}\right)^{\eta} s_i\,|a_i|^2\right], \text{ and}$$
$$\mathbb{E}[P_N] = \overline{\sigma}^2, \tag{1}$$

Since the log-distance path loss, the spatially-correlated shadowing and the multipath fading are mutually independent, $\mathbb{E}[P_{RX}]$ can be expressed as

$$\mathbb{E}[P_{RX}] = \overline{P_{TX}}\mathbb{E}\left[\left(\frac{d_0}{d_i}\right)^{\eta}\right]\mathbb{E}[s_i]\,\mathbb{E}\left[|a_i|^2\right], \tag{2}$$

with $\mathbb{E}\left[|a_i|^2\right] = 1$. From [9], we have

$$\mathbb{E}\left[\left(\frac{d_0}{d_i}\right)^{\eta}\right] = \frac{1}{\pi r^2 d_0^{-\eta}} \int_0^{2\pi}\int_0^{r}\Big[(z\,\cos\theta - PU_x)^2 + (z\,\sin\theta - PU_y)^2\Big]^{-\frac{\eta}{2}} z\; dz\; d\theta, \tag{3}$$

$$\mathbb{E}[s_i] = \exp\left(\frac{{\sigma_s^{\text{dB}}}^2 \ln^2(10)}{200}\right). \tag{4}$$

In the case of Model 2, it follows that

$$\text{SNR}_2 = \mathbb{E}\left[\frac{P_{RX}}{P_N}\right] = \mathbb{E}[P_{RX}]\mathbb{E}\left[\frac{1}{\sigma^2}\right], \tag{5}$$

since the received signal and noise are independent. The first term is equivalent to the upper term of SNR Model 1, and the second term is [9]

$$\mathbb{E}\left[\frac{1}{\sigma^2}\right] = \begin{cases} \frac{1}{\overline{\sigma}^2} & \text{for } \rho = 0 \\ \frac{1}{2\overline{\sigma}^2\rho}\ln\left(\frac{1+\rho}{1-\rho}\right) & \text{for } 0 < \rho < 1 \end{cases}. \tag{6}$$

The different models affect the system in the sense that they are used to link the average noise power and other parameters, like transmitted power, to establish a predefined SNR condition on computer simulations and analytical derivations.

The desired average signal-to-noise ratio, $\overline{\text{SNR}}$, for both models can be obtained by making the transmitted power constant, evaluating $\mathbb{E}[P_{RX}]$ using expressions (2)-(4) and calculating the average signal noise power as

$$\overline{\sigma}^2_{\text{SNR1}} = \frac{\mathbb{E}[P_{RX}]}{\overline{\text{SNR}}}, \tag{7}$$

$$\overline{\sigma}^2_{\text{SNR2}} = \frac{\mathbb{E}[P_{RX}]}{\overline{\text{SNR}}}, \tag{8}$$

$$\overline{\sigma}^2_{\text{SNR2}} = \frac{\mathbb{E}[P_{RX}]}{\overline{\text{SNR}}}\frac{1}{2\rho}\ln\left(\frac{1+\rho}{1-\rho}\right) \tag{9}$$

for SNR Model 1, for SNR Model 2 and $\rho = 0$, or for SNR Model 2 and $0 < \rho < 1$, respectively. This will make the average noise power to be adjusted, so that when the noise is added to the received signal, the resulting SNR is the intended.

E. Detectors and Data Fusion Scheme

The system model is modular and flexible, allowing the assessment of both Cooperative Spectrum Sensing (CSS), with m matching the number of SUs, and Non-Cooperative Spectrum Sensing (NCSS), with $m = 1$. Since the main interest resides where the noise power is a random variable, and in the system model this is the case when $m > 1$ and $\rho \neq 0$, only CSS is considered herein.

In centralized CSS with data fusion, the matrix $\mathbf{X}$ is processed by the Fusion Center (FC) to calculate the test statistic for the specific detection algorithm chosen.

For the blind detectors assessed in this article, the sample covariance matrix (SCM) of the received signal is computed as $\mathbf{R} = \frac{1}{n}\mathbf{X}\mathbf{X}^{\dagger}$ with $|\cdot|^{\dagger}$ denoting the conjugate and transposition operation.

The expressions below summarizes the test statistics employed by the CSS schemes adopted in this article, where: $r_{i,k}$ is the element on the ith row and jth column of $\mathbf{R}$, r_i is the ith element of the vector $\mathbf{r}$ formed by stacking all rows of $\mathbf{R}$, $\overline{r}$ is the mean value of r_i, $0 \leq \epsilon \neq 1$ is the inequality aversion parameter, det($\mathbf{R}$) is the determinant of $\mathbf{R}$, $\mathbf{E}$ is the diagonal matrix in which the elements $e_{i,i}$ are the Euclidean norm of the ith row of $\mathbf{R}$, $\lambda_1 \geq \lambda_2 \geq \dots \geq \lambda_m$ are the eigenvalues of $\mathbf{R}$, and $c_{i,j}$ are the elements of the matrix $\mathbf{C} = \mathbf{D}^{-\frac{1}{2}}\mathbf{R}\mathbf{D}^{-\frac{1}{2}}$, with $\mathbf{D}$ being the diagonal matrix with elements$_{i,i} = r_{i,i}$. The detectors' names are: Gini index detector (GID) [10], Pietra-Ricci index detector (PRIDe) [11], Atkinson index detector (AID) [12], Hadamard ratio (HR) detector [13], volume-based detector number 1 (VD1) [14], scaled largest eigenvalue (SLE) detector [15], arithmetic-to-geometric mean (AGM) detector [16], maximum-minimum eigenvalue detector (MMED) [15], locally most powerful invariant test (LMPIT) detector [17], and mean-to-square extreme eigenvalue (MSEE) detector [3].

$$T_{\text{GID}} = \frac{\sum_{i=1}^{m^2}|r_i|}{\sum_{i=1}^{m^2}\sum_{j=1}^{m^2}|r_i - r_j|}, \qquad T_{\text{PRIDe}} = \frac{\sum_{i=1}^{m^2}|r_i|}{\sum_{i=1}^{m^2}|r_i - \overline{r}|},$$

$$T_{\text{AID}} = \frac{1}{\overline{r}}\left(\sum_{i=1}^{m}\sum_{j=1}^{m} r_{i,j}^{1-\epsilon}\right)^{\frac{1}{1-\epsilon}}, \quad T_{\text{MMED}} = \frac{\lambda_1}{\lambda_m},$$

$$T_{\text{AGM}} = \frac{\frac{1}{m}\sum_{i=1}^{m}\lambda_i}{\left(\prod_{i=1}^{m}\lambda_i\right)^{\frac{1}{m}}}, \qquad T_{\text{HR}} = \frac{\det(\mathbf{R})}{\prod_{i=1}^{m} r_{i,i}},$$

$$T_{\text{SLE}} = \frac{\lambda_1}{\sum_{i=1}^{m}\lambda_i}, \qquad T_{\text{VD1}} = \log\left[\det\left(\mathbf{E}^{-1}\mathbf{R}\right)\right],$$

$$T_{\text{LMPIT}} = \sum_{i=1}^{m}\sum_{j=1}^{m}|c_{i,j}|^2, \quad T_{\text{MSEE}} = \frac{\lambda_1+\lambda_m}{2\sqrt{\lambda_1\lambda_m}}.$$

III. Simulation Results

This section presents the simulation results evaluating how the two SNR models affect the performance assessment of the listed detectors. Table I describes the standard parameter values used in the simulations, except when otherwise explicitly specified. In spite of the SNR being a result of a set of predefined system parameter, it was used to calculate $\overline{\sigma}^2$, in order to ensure a desired signal-to-noise ratio on the simulations. This was done using expressions (7)-(9), depending on the SNR model under consideration. The value of $\overline{\sigma}^2$ was the only difference between simulations carried out to evaluate the performance of the detectors according to each SNR model.

TABLE I: System parameters and standard values used in simulations.

Symb.	Description	Value
r	SU operation area (OA) radius	1 km
$PU_{(x,y)}$	Position of the PU from SU OA center	(1,1) km
m	Number of SUs	5
n	Number of received samples per SU $m > 1$	400
η	Path loss exponent	2.5
d_0	Path loss model reference distance	1 m
μ_k	Rice factor mean value	1.88 dB
σ_k	Rice factor standard deviation	4.13 dB
σ_s	Shadowing standard deviation	7 dB
$\overline{\sigma}^2$	Average receiver noise power	-28.9 dBm
v	Number of row/columns of $\mathbf{\Sigma}$, $\mathbf{S_c}$ and $\mathbf{S_u}$	50
Λ	Shadowing spatial correlation length	25
P_{TX}	PU signal power at d_0	5 W
N_s	Number of samples per modulated symbol	3
ρ	Noise level power variation parameter	0.99
P_{fa}	Reference probability of false alarm	0.1
ϵ	Inequality aversion parameter of the AID	0.1

Fig. 1 shows the analytical and measured values of SNR, evaluated using Models 1 and 2. The analytical results was obtained using equations (1)-(4) for Model 1 and equations (2)-(6) for Model 2. The simulation performed an ensemble of 10000 iterations and the results were averaged. The parameter set presented in Table I was adopted, except for ρ which varied from 0 to 0.99.

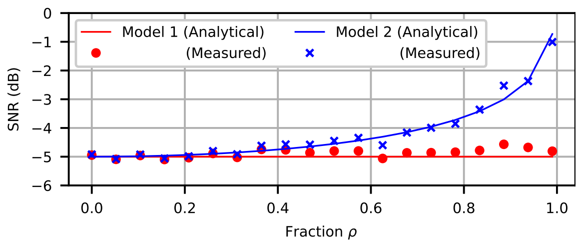

Fig. 1: Analytical and simulated SNR values for both models versus ρ.

As expected, for $\rho = 0$ both models lead to the same SNR, since in this case the noise power is deterministic and equal to $\overline{\sigma}^2$. Being the signal power random due to system model, this fits in the third scenario presented in Section I-B.

As ρ increases, noise power becomes random, fitting in the first scenario described in the problem description. The result is a constant SNR calculated using Model 1, and an increasing SNR when Model 2 is applied, with $\text{SNR}_2 \geq \text{SNR}_1$, as stated in Section I-B.

This can be explained by the fact that the SNRs evaluated using Models 1 and 2 for $0 < \rho < 1$ differ by a factor of $\frac{1}{2\rho}\ln\left(\frac{1+\rho}{1-\rho}\right)$, which increases with ρ. For $\rho = 0.99$, used in the remaining of the simulations, this difference is equal to 4.27 dB, enough to produce relevant discrepancies on the detectors' performance results, as shown bellow.

To better illustrate those discrepancies, Fig. 2 displays the probability of detection P_d for the evaluated detectors, under the standard parameter set from Table I, except for a targeted SNR varying from -15 to 5 dB. In spite of small variations on the curve shapes due to particular simulation iterations, the graph for SNR Model 2 can be seen as the one for SNR Model 1 shifted to the right by the amount of 4.27 dB in the SNR axis.

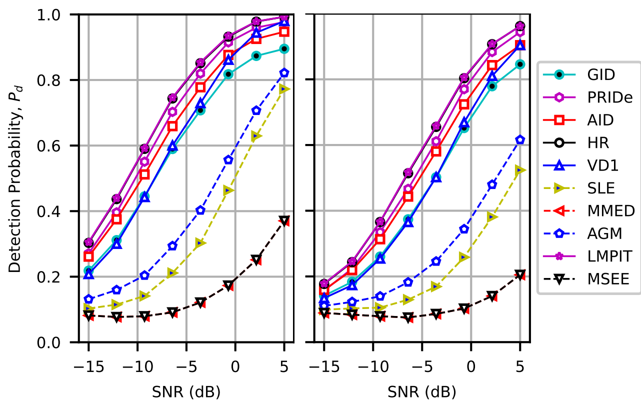

Fig. 2: Detection probability, P_d, for the standard parameter set, over targeted SNR varying from -15 to 5 dB for SNR Model 1 (left) and Model 2 (right).

This is due to the fact that (9) produces higher average noise power than (7), and, as a consequence, the detectors suffer more from noise effects when SNR Model 2 is applied. This can falsely lead to a better detector performance perception when using SNR Model 1.

Additionally, certain detector performance characteristics could be neglected in different simulation circumstances, like in Fig. 3. Using SNR Model 1, it appears that the LMPIT and the HR detectors are not affected when ρ is increased, but they rather improve their performances. It also looks like GID, PRIDe, AID and VD1 are less affected. On the other hand, in Fig. 3 (right) it can be seen that they all lose performance in a much greater extent.

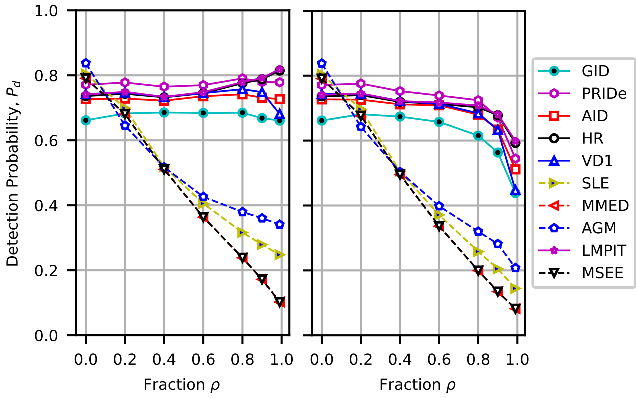

Fig. 3: Detection probability, P_d, for the standard parameter set, for $0 \leq \rho < 1$ for SNR Model 1 (left) and Model 2 (right).

This is explained by the fact that, as shown in Fig. 1, if $\overline{\sigma}^2$ is kept constant while increasing ρ, the SNR increases if Model 2 is taken into account, which in consequence makes the probability of detection increase, a behavior also noted in Fig. 2. To keep the SNR constant, the average noise power $\overline{\sigma}^2$ also needs to be increased, which degrades more the received signal and lowers the detection probabilities.

Fig. 4 shows a case in which the detectors LMPIT and HR are compared using a combination of the SNR models. The probability of detection under standard system parameters for varying η is plotted for both detectors. On the left-side graph, the detectors' performances were evaluated using SNR Model 1 for LMPIT, and Model 2 for HR. In this case, LMPIT performs much better than HR. The center graph displays an opposite result, with LMPIT being evaluated using SNR Model 2, while HR applies Model 1.

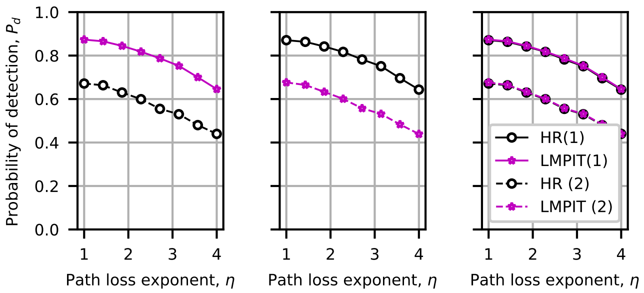

Fig. 4: SNR Model mismatch comparison for LMPIT and HR detectors, using SNR Models 1 and 2 respectively, on the left, 2 and 1 on center, and all models on the right, under standard simulation parameter set, for varying η.

In fact, when the same SNR model is used for both detectors, their performances are found to be virtually the same, as shown in Fig. 4, right. It is also noteworthy that the detection probabilities for the SNR Model 1 are higher than for Model 2 for both detectors, due to already discussed reasons.

IV. Conclusions

This paper examined how different SNR modeling approaches affect the performance evaluation of spectrum sensing detectors. Using analytical expressions and simulation-based analysis, we showed that even under the same signal and channel conditions, the use of different SNR models - specifically when the noise is random - can result in substantially different average SNR values.

These differences, in turn, influence key performance metrics such as the detection probability, potentially leading to biased comparisons among spectrum sensing algorithms. Our findings underline the importance of explicitly defining and justifying the chosen SNR model when designing or evaluating cognitive radio systems.

Notably, we found that many published works fail to specify which SNR model is used, which hampers the reproducibility and fair comparison of results across studies. To address this, we also provided an open-source simulation code to encourage transparency and standardized benchmarking.

Future work may explore the behavior of the SNR models in scenarios where the signal and noise are not independent or when both follow correlated or non-Gaussian distributions. Additionally, developing guidelines or toolkits to standardize SNR modeling in simulation frameworks could significantly improve consistency in spectrum sensing research.

References

[1] R. Tandra and A. Sahai, "SNR wall for signal detection," *IEEE J. Sel. Topics Signal Process.*, vol. 2, no. 1, pp. 4–17, 2008.

[2] H. Huang and C. Yuan, "Cooperative spectrum sensing over generalized fading channels based on energy detection," *China Commun.*, vol. 15, no. 5, pp. 128–137, 2018.

[3] K. Bouallegue, I. Dayoub, M. Gharbi, and K. Hassan, "Blind spectrum sensing using extreme eigenvalues for cognitive radio networks," *IEEE Commun. Lett.*, vol. 22, no. 7, pp. 1386–1389, 2018.

[4] W. Ejaz, N. U. Hasan, and H. S. Kim, "Snr-based adaptive spectrum sensing for cognitive radio networks," *Int. J. Innov. Comput. Inf. Control*, vol. 8, 2012.

[5] N. I. Miridakis, T. A. Tsiftsis, and G. Yang, "Moment-based spectrum sensing under generalized noise channels," *IEEE Commun. Lett.*, vol. 25, no. 1, pp. 89–93, 2021.

[6] H. A. Tageldien, R. Mounir, M. Tantawy, and H. Abdel-Kader, "Noise uncertainty effect on a modified two-stage spectrum sensing technique," *Indones. J. Electr. Eng. Comput. Sci.*, vol. 1, no. 2, pp. 341–348, 2016.

[7] A. Halaki, S. Sarkar, S. Gurugopinath, and M. Rangarao, "Norm-based spectrum sensing for cognitive radios under generalised gaussian noise," *IET Netw.*, vol. 12, pp. 282–294, 2023.

[8] I. Ramírez, D. Martinez, A. Andrade, G. Galaviz, and N. Barboza, "Spectral minima tracking for improving the energy detection under noise power uncertainty," *Alexandria Eng. J.*, vol. 66, 2022.

[9] D. A. Guimarães, "Income inequality index detectors for non-cooperative spectrum sensing in cognitive communications," *IEEE Trans Cognit Commun Networking(submitted)*, 2025.

[10] ——, "Modified gini index detector for cooperative spectrum sensing over line-of-sight channels," *Sensors*, vol. 23, no. 12, 2023.

[11] D. A. Guimarães, E. J. T. Pereira, and R. Shrestha, "Resource-efficient low-latency modified Pietra-Ricci index detector for spectrum sensing in cognitive radio networks," *IEEE Trans. Veh. Technol.*, vol. 72, no. 9, 2023.

[12] D. A. Guimarães, "Atkinson index detector for spectrum sensing," *J. Commun. Inf. Syst.*, vol. 39, no. 1, pp. 189–193, 2024.

[13] L. Huang, Y.-H. Xiao, H. C. So, and J. Fang, "Accurate performance analysis of hadamard ratio test for robust spectrum sensing," *IEEE Trans. Wireless Commun.*, vol. 14, no. 2, pp. 750–758, 2015.

[14] L. Huang, C. Qian, Y.-H. Xiao, Q. T. Zhang, and Q. Zhang, "Performance analysis of volume-based spectrum sensing for cognitive radio," *IEEE Trans. Wireless Commun.*, vol. 14, no. 1, pp. 317–330, 2015.

[15] B. Nadler, F. Penna, and R. Garello, "Performance of eigenvalue-based signal detectors with known and unknown noise level," in *Proc. IEEE Int. Conf. Commun. (ICC)*, 2011.

[16] R. Zhang, T. J. Lim, Y.-C. Liang, and Y. Zeng, "Multi-antenna based spectrum sensing for cognitive radios: A GLRT approach," *IEEE Trans. Commun.*, vol. 58, no. 1, pp. 84–88, 2010.

[17] D. Ramírez, J. Via, I. Santamaria, and L. L. Scharf, "Locally most powerful invariant tests for correlation and sphericity of gaussian vectors," *IEEE Trans. Inf. Theory*, vol. 59, no. 4, pp. 2128–2144, 2013.